Journal of Molecular Graphics and Modelling 54 (2014) 46–53

Contents lists available at ScienceDirect

Journal of Molecular Graphics and Modelling

journal homepage: www.elsevier.com/locate/JMGM

Predicting the structures of complexes between phosphoinositide 3-kinase (PI3K) and romidepsin-related compounds for the drug design of PI3K/histone deacetylase dual inhibitors using computational docking and the ligand-based drug design approach

Akifumi Oda[a,b,c,*], Ken Saijo[d], Chikashi Ishioka[d], Koichi Narita[b], Tadashi Katoh[b], Yurie Watanabe[a], Shuichi Fukuyoshi[a], Ohgi Takahashi[b]

[a] Institute of Medical, Pharmaceutical and Health Sciences, Kanazawa University, Kakuma-machi, Kanazawa 920-1192, Ishikawa, Japan
[b] Faculty of Pharmaceutical Sciences, Tohoku Pharmaceutical University, 4-4-1 Komatsushima, Aoba-ku, Sendai 981-8558, Miyagi, Japan
[c] Institute for Protein Research, Osaka University, 3-2 Yamadaoka, Suita 565-0871, Osaka, Japan
[d] Institute of Development, Aging and Cancer, Tohoku University, 4-1 Seiryo-machi, Aoba-ku Sendai 980-8575, Miyagi, Japan

ARTICLE INFO

Article history:
Accepted 30 August 2014
Available online 8 September 2014

Keywords:
Phosphoinositide 3-kinase
Romidepsin
Dual inhibitor
Computational docking
Molecular superposition
Molecular dynamics simulation

ABSTRACT

Predictions of the three-dimensional (3D) structures of the complexes between phosphoinositide 3-kinase (PI3K) and two inhibitors were conducted using computational docking and the ligand-based drug design approach. The obtained structures were refined by structural optimizations and molecular dynamics (MD) simulations. The ligands were located deep inside the ligand binding pocket of the p110α subunit of PI3K, and the hydrogen bond formations and hydrophobic effects of the surrounding amino acids were predicted. Although rough structures were obtained for the PI3K–inhibitor complexes before the MD simulations, the refinement of the structures by these simulations clarified the hydrogen bonding patterns of the complexes.

1. Introduction

Phosphoinositide 3-kinase (PI3K) is the enzyme that phosphorylates the 3′-OH group of the inositol ring in phosphatidylinositol 4,5-bisphosphate, which is located in the cell membrane, to generate phosphatidylinositol 3,4,5-trisphosphate; this kinase is a component of the PI3K/Akt pathway [1]. PI3K consists of a heterodimer with a catalytic and a regulatory subunit. A relationship has been detected between mutations of *PIK3CA*, which encodes the catalytic subunit p110α, and several human cancers [2]. The activation of the PI3K/Akt pathway is likely to play important roles in carcinogenesis and cancer progression; therefore, PI3K inhibitors are considered as promising agents for anticancer treatments. Clinical trials of PI3K inhibitors have been conducted, and the efficacies of these inhibitors in the treatment of progressive cancer have been investigated [3]. PI3K is a probable drug target; however, no PI3K inhibitors currently exist on the market, and the development of compounds with high activity and safety is desirable.

Previously, we constructed an assay system to evaluate the inhibitory activities of PI3K inhibitors using a strain of the yeast *Saccharomyces cerevisiae* with deleterious mutations in the ATP-binding cassette transporter genes [4]. Using our assay system, we screened the chemical library of the Screening Committee of Anticancer Drugs supported by a Grant-in-Aid for Scientific Research on Innovative Areas and Scientific Support Programs for Cancer Research from the Ministry of Education, Culture, Sports, Science and Technology, Japan. This screening indicated the histone deacetylase (HDAC) inhibitor romidepsin (FK-228) [5,6] and its analogs as likely inhibitors of PI3K. Fig. 1 displays romidepsin and FK-A5, the PI3K inhibitory activity of which was the highest of all romidepsin analogs. Key atoms are named in the figure for reference in the following discussion. The IC_{50} values for PI3K of romidepsin and FK-A5 were 57.1 μM and 26.2 μM, respectively. In addition, the IC_{50} values for HDAC1 of romidepsin and FK-A5 were 3.6 nM and 2.5 nM, respectively. Because the inhibition of HDAC6 possibly causes cardiac toxicity, selective inhibition for HDAC1 is desirable for HDAC inhibitors. Romidepsin and its analogs are highly selective inhibitors for HDAC1. The cytocidal effects of these

* Corresponding author at: Kanazawa University, Faculty of Pharmacy, Institute of Medical, Pharmaceutical and Health Sciences, Kakuma-machi, Kanazawa, Japan. Tel.: +81 76 234 4485; fax: +81 76 234 4485.
E-mail address: oda@p.kanazawa-u.ac.jp (A. Oda).

http://dx.doi.org/10.1016/j.jmgm.2014.08.007
1093-3263/

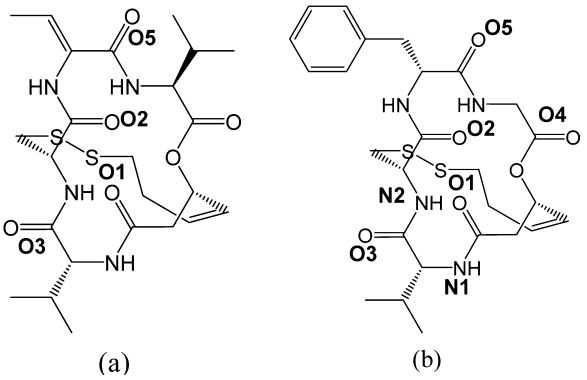

Fig. 1. PI3K/HDAC dual inhibitors found by our team. (a) Romidepsin (b) FK-A5.

compounds have also been investigated, and romidepsin and its analogs have been found to be effective in HDAC inhibitor–resistant cells.

HDAC is the enzyme that catalyzes the histone deacetylation reaction. Because the enzyme plays an important role in transcriptional regulation, HDAC is considered to be a promising target for anticancer drugs [7]. Romidepsin was developed as an HDAC inhibitor, and it was approved by the FDA for the treatment of cutaneous T-cell lymphoma (CTCL) and peripheral T-cell lymphoma (PTCL). HDAC inhibitors other than romidepsin have also been developed, resulting in several currently marketed drugs and promising drug candidates [8]. Tumor shrinkage and symptomatic improvements have been observed due to the use of these compounds. In addition, the adhibition of romidepsin for diseases other than CTCL and PTCL, e.g., multiple myeloma and kidney cancer, is under investigation. Moreover, the use of a PI3K inhibitor and an HDAC inhibitor in combination has been reported to enhance the cytocidal effect [9–11]; therefore, the development of a PI3K/HDAC dual inhibitor would represent a significant advance in the treatment of intractable cancer. Because of the drug resistance of cancer cells, multiagent chemotherapy and/or multitarget drugs are particularly useful. For several multikinase inhibitors such as sorafenib [12], which is used for the treatment of kidney cancer and hepatocarcinoma, favorable outcomes have been reported. Thus, multitarget drugs are considered to be effective for anticancer treatment. Although a PI3K/HDAC dual inhibitor would be a promising anticancer agent, the PI3K inhibitory activities of previously developed compounds are much less than their HDAC inhibitory activities. High inhibition of both PI3K and HDAC is desirable in the development of effective PI3K/HDAC dual inhibitors.

Structural modification of drug candidates using rational drug design techniques [13] is useful for improving drug activity. Rational drug design is a structure-based drug design (SBDD) procedure in which the modification of the drug's structure is conducted in reference to the three-dimensional (3D) structure of the complex between the drug target and the ligand molecule. For example, steric crash in the complex can be removed, or empty space filled by removing bulky substituents from or adding them to the ligand molecule, respectively. For the modification of a ligand molecule by SBDD, a 3D structure of the target–ligand complex is indispensable; however, experimentally determined complex 3D structures are frequently unavailable at the early stages of drug design. Indeed, the 3D structure of the PI3K–romidepsin complex has not been experimentally observed. If the structure of a complex has not been determined experimentally, it should be predicted by computational docking [14]. In computational docking, the interaction pattern between the protein and the ligand is predicted, and the conformation and the configuration of the ligand (docking pose) are determined in silico. Docking calculations consist of two steps, i.e., docking and scoring. The candidate structures of the protein–ligand complex are predicted in the docking step, and the candidates are evaluated in the scoring step. At present, although reasonable structures can be obtained for the complexes of many protein–ligand systems in the docking step, evaluating these predicted structures in the scoring step is occasionally difficult because of the difficulties in calculating binding free energy. To solve this problem, improvements to these scoring functions such as consensus scoring [15] have been developed. Additionally, several techniques other than SBDD methods may be combined with computational docking in some cases. For example, enzymatic reaction mechanisms are useful for selecting the docking poses of protein–substrate systems. Complex structures may also be predicted by reference to other complexes whose 3D structures are already known. Furthermore, ligand-based drug design (LBDD) techniques, which constitute another class of in silico drug design methods, can be combined with computational docking to construct appropriate models for protein–ligand complexes [16].

The concept of LBDD is that information about known active compounds may be used for the developments of novel compounds [17]. The major techniques of LBDD are quantitative structure-activity relationship studies and pharmacophore searches. Although LBDD uses only information about known ligands, the method hypothesizes that similar compounds dock into drug targets by similar binding modes. Thus, the formation of protein–ligand complexes is also considered in LBDD, as it is in SBDD. Many LBDD techniques require the superposition of known ligands to predict the binding conformations of ligands in the protein–ligand complex. If similar compounds are accurately superposed with large overlap, the conformations of these ligands may be considered as candidate binding conformations. Therefore, LBDD techniques can help predict protein–ligand complex structures from a different theoretical standpoint than SBDD procedures.

In this study, the 3D structures of the complexes between PI3K and two inhibitors, i.e., romidepsin and its analog, were predicted using a combination of computational docking and molecular superposition. Although we have previously performed rough docking calculations for the binding of romidepsin with PI3K [4], detailed investigations of the binding mode and binding affinity were not conducted. This previous docking model only indicated the competitive inhibition of romidepsin for PI3K. In the present study, because docking calculations were conducted not only for romidepsin but also for a romidepsin analog (FK-A5), a detailed model could be obtained that explained the activities of these compounds. In addition, molecular dynamics (MD) simulations of the predicted structures of the complexes were conducted to refine their 3D structures.

2. Material and methods

In this study, the 3D structure of PI3K extracted from the Protein Data Bank [18] (PDB ID: 3HHM) was used as the target structure for the docking calculations. Because this entry represented the 3D structure of the tertiary complex among the catalytic subunit p110α, the regulatory subunit p85α and the inhibitor wortmannin [19], a complex between p110α and p85α constructed by removing wortmannin was used for docking. The location of wortmannin in the tertiary complex was defined as the ligand binding site of PI3K. The ligands used in this study were romidepsin and FK-A5, the structures of which are illustrated in Fig. 1. For the ligand structures, the disulfide bonds were broken and the thiol form molecules were used because of the reductive environment of the human body. The ligand geometries were obtained by hybrid density functional theory B3LYP/6-311G(df, p) using Gaussian 03 [20].

Protein–ligand docking calculations were conducted using FRED [21]. Because FRED is a rigid docking program in which ligand conformations are not changed during the docking calculations, conformation generation methods must be used in conjunction with the program. The conformation generation program OMEGA [22] is generally used with FRED. Although OMEGA is a fast and effective conformation generator, its search of the conformational space of macrocyclic molecules such as romidepsin may be insufficient because the ring conformations of these molecules are taken from the program's fragment library. Therefore, preliminary conformational searches were conducted before the OMEGA calculations to search the conformational spaces of romidepsin and FK-A5 extensively. LMOD [23] was used for the preliminary conformational searches in this study, and additional conformational searches by OMEGA were conducted for the conformations generated by LMOD. LMOD is a conformational search algorithm based on the eigenvector following of low-frequency vibrational modes. Because the algorithm is based on physicochemical concepts, LMOD is expected to be effective for use in combination with OMEGA, which is based on a different theoretical framework. For the conformational search by LMOD, the general AMBER force field (GAFF) [24] was adopted. The number of conformations to store in conflib was set to 400, and the energy window for conformation storage was set to 50 kcal/mol. The minimizations were terminated when the energy gradient was less than 0.2 kcal/mol Å. In the OMEGA calculations performed after the LMOD search, the setting "-fromCT false", in which the initial conformations are used for the conformational search, was adopted. Although only the connection table is used and the initial coordinates do not influence the search results in the default setting of OMEGA, the initial coordinates were used for the OMEGA calculations in the present study to utilize the results of the LMOD search. The number of generated conformations was set to 100 for each OMEGA calculation. Because the preliminary calculations using LMOD generated 12 and 14 conformations for romidepsin and FK-A5, respectively, the final numbers of generated conformations were 1200 and 1400 for romidepsin and FK-A5, respectively.

Docking calculations were conducted for all conformations using the rigid docking program FRED 3.0.0. Thus, the numbers of generated docking poses were 1200 and 1400 for romidepsin and FK-A5, respectively. In the FRED calculations, dock_resolution was set to high. Because similar docking poses were included in the pose ensembles, representative docking poses were extracted using clustering. For the clustering calculations, two docking poses were placed in the same cluster when the root mean square deviation (RMSD) between them was less than 1.0 Å. After clustering, representative conformations, the FRED docking scores (Chemgauss4) of which were the lowest in their clusters, were extracted. The numbers of representative docking poses were 31 and 124 for romidepsin and FK-A5, respectively.

The structures of romidepsin and FK-A5 are similar, as shown in Fig. 1, and both compounds inhibit PI3K. Thus, the structures of the complexes of these compounds with PI3K were also expected to be similar. According to this presumption, the representative docking poses of romidepsin and FK-A5 were exhaustively superposed, and a pair of docking poses with high similarity was selected. That is, if one of the docking poses of romidepsin and one of the poses of FK-A5 were similar, these poses were considered as promising candidates for the actual PI3K-inhibitor 3D structures. The superposition of the poses and the similarity calculations were conducted using ROCS [25]. For the evaluations of pose similarity, TanimotoCombo, which represents the sum of the similarity of molecular shape (ShapeTanimoto) and the similarity of molecular properties (ColorTanimoto), was used. The superposition of docking poses was exhaustively conducted for all combinations of the representative docking poses, i.e., $31 \times 124 = 3844$ patterns. Using these superposition calculations, similar docking poses for romidepsin and FK-A5 were selected, and they were considered as the final candidate structures of the PI3K–inhibitor complexes. A flowchart of the calculations is shown in Fig. 2.

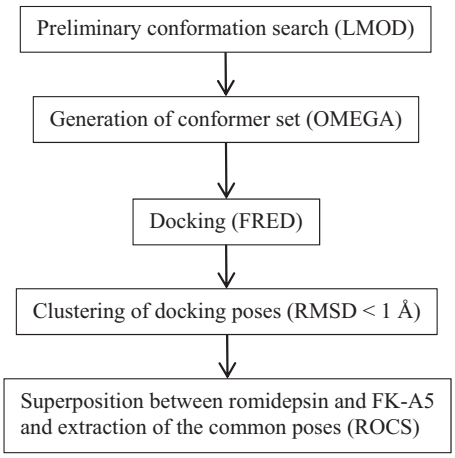

Fig. 2. Flowchart of the prediction of the structures of the complexes between PI3K and the inhibitors.

MD simulations of the structures of the complexes generated by the docking calculations and the molecular superposition were conducted for their further refinement. For the MD simulations, the TIP3P water solvent model with a thickness of at least 8 Å was used, and sodium ions were added as counterions. Arg1047 was substituted by His. At first, structural minimizations of the complexes were conducted, followed by temperature-increase MD simulations to 300 K with the fixed protein. After the temperature-increase MD simulations, equilibration MD simulations at 300 K were performed. For the minimizations, 5000 steps for the water, counterions and ligands were conducted, followed by 10,000 steps for the whole systems. For the MD simulations, 30 ps and 5 ns simulations were performed for the temperature-increase and equilibration simulations, respectively, and the time step of the MD simulations was set to 1 fs. The covalent bonds containing hydrogen atoms were restricted by SHAKE. The system, including an explicit solvent model, was simulated with a periodic boundary condition, and the particle mesh Ewald method was employed to treat long-range electrostatic interactions. A cutoff of 10 Å was used for nonbonding interactions. Finally, 10,000 steps were conducted for the minimization of the structures of the complexes obtained by the MD simulations. The force field parameters for the protein were ff99SB [26,27], and those for inhibitors were GAFF. The minimizations and MD simulations were conducted using AMBER12 and AmberTools12 [28]. Using the last 4 ns trajectories generated by the MD simulations, binding free energies between PI3K and inhibitors were calculated by the molecular mechanics/generalized born surface area (MM/GBSA) method. Snapshots were picked up every 50 ps, and the default settings were used for the MM/GBSA calculations. In addition, MD simulation for the PI3K–wortmannin complex (PDB ID: 3HHM) was conducted using the aforementioned procedures for comparison.

3. Results and discussion

As previously mentioned, 31 and 124 poses were obtained by the docking calculations for romidepsin and FK-A5, respectively. Through the superposition of these poses, one pair of docking poses whose TanimotoCombo value was larger than 0.8 (0.804) was selected. The selected 3D structure for the PI3K–romidepsin complex is shown in Fig. 3a, and the superposition of romidepsin and FK-A5 is illustrated in Fig. 3b. The TanimotoCombo value of this

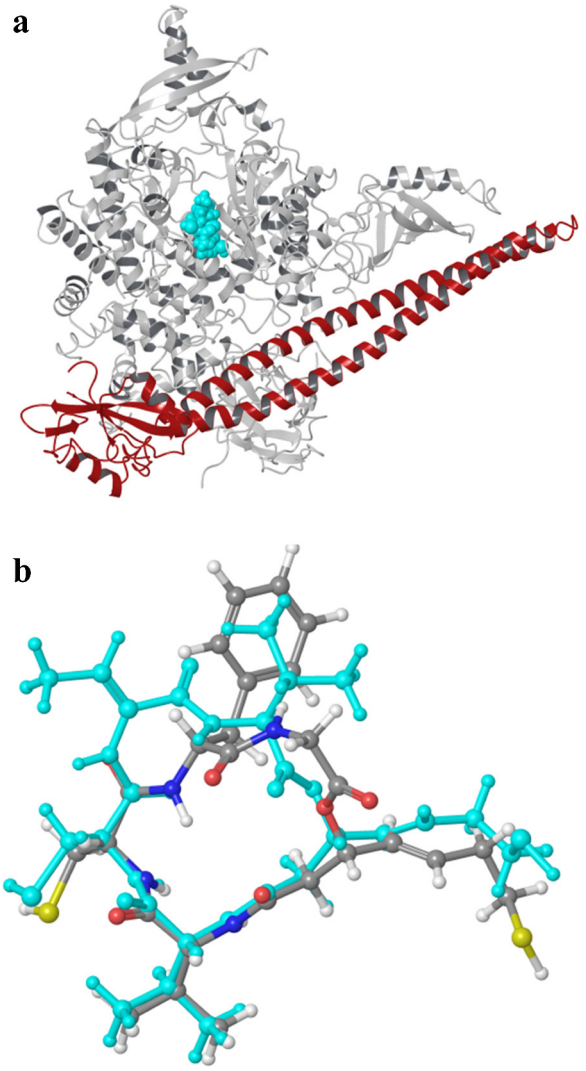

Fig. 3. Predicted docking poses. (a) PI3K-romidepsin complex. White and red ribbons indicate the p110α and p85α subunits, respectively. The light blue molecule is romidepsin. (b) The ligand structures in the complex. Romidepsin (light blue) and FK-A5 (colored by element).

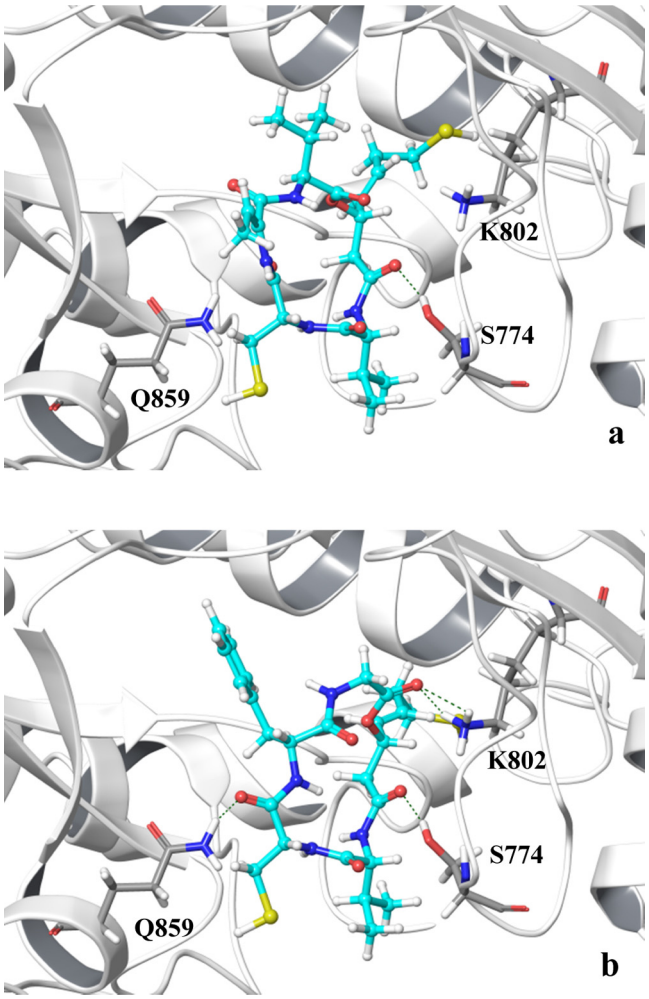

Fig. 4. Hydrogen bonds between PI3K and the ligands in the complexes. The green dashed lines indicate the hydrogen bonds. (a) PI3K-romidepsin (b) PI3K–FK-A5 complexes. (For interpretation of the references to color in this figure legend, the reader is referred to the web version of this article.)

pair was the best of all pairs. In addition, because the ShapeTanimoto values were larger than the ColorTanimoto values for all pairs, auto-scaled ShapeTanimoto and ColorTanimoto values were calculated and compared. Not only for the TanimotoCombo values but also for the average values of the auto-scaled ShapeTanimoto and ColorTanimoto values, which are as used in one of the consensus scoring strategies named AASS [15], the selected pair shown in Fig. 3a and b was the best. These poses, as ranked by their Chemgauss4 score values, represent the 18th of 31 poses for romidepsin and the 16th of 124 poses for FK-A5. Before clustering, these poses were ranked 562nd of 1200 and 275th of 1400 for romidepsin and FK-A5, respectively. The Chemgauss4 score values of the selected poses were −4.33 and −5.20 for romidepsin and FK-A5, respectively (Chemgauss4 is a dimensionless quantity). Of all 1200 poses for romidepsin, the best score was −6.17 and the worst was −2.26. For all 1400 poses of FK-A5, the best score was −6.84 and the worst was −0.77. Therefore, the poses selected by the combination of docking and superposition were ranked as superior or medium among the docking poses in terms of Chemgauss4 score. As shown in Fig. 3a, the ligand was located in the kinase pocket of the p110α subunit of PI3K, as was consistent with the experimental results of the competitive inhibitory activities for romidepsin and its analogs. In addition, the macrocyclic structures in the docking poses of romidepsin and FK-A5 were highly overlapped (Fig. 3b). The atoms around the 21-isopropyl and the adjoining amides were particularly well superposed, indicating that this position plays an important role in the interactions between romidepsin or its analogs and PI3K. In addition, the 4-isopropyl of romidepsin and the 7-benzyl of FK-A5 were superposed. Because both of these substituents are hydrophobic, the results indicate that the hydrophobic effects of these positions play significant roles in the inhibitory activities of romidepsin and its analogs. The locations of the two thiol groups generated through the reduction of the disulfide bonds were not as well conserved in the two inhibitors as were the locations of the adjacent atoms of 21-isopropyl. Although the thiol moiety is considered to be important for the interactions between HDAC and romidepsin [29], it may be not significant for the compound's interactions with PI3K, which possesses no metal ions in its catalytic site.

In Fig. 4, the hydrogen bonds between PI3K and romidepsin (Fig. 4a) and between PI3K and FK-A5 (Fig. 4b) in the predicted structures of the complexes are illustrated. The definition of hydrogen bond was as follows: the distance between hydrogen and the acceptor atom is shorter than or equal to 3.0 Å, and the angle is larger than or equal to 90°. As shown in the figure, only Ser774 formed a hydrogen bond with romidepsin, while Ser774, Gln859 and Lys802 all formed hydrogen bonds with FK-A5. The results of

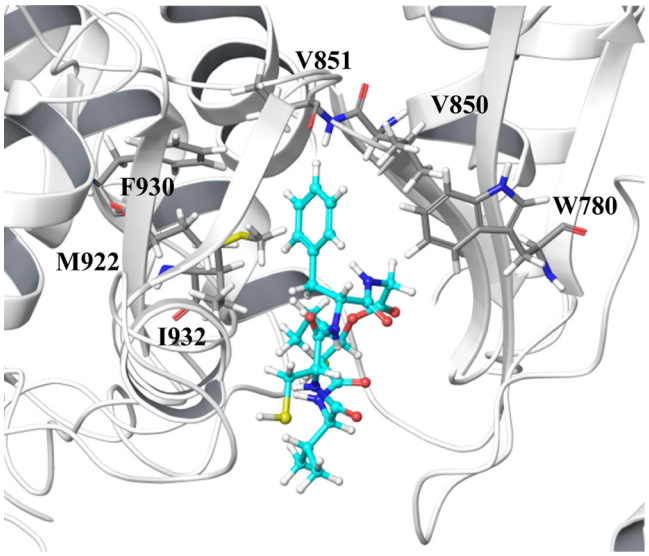

Fig. 5. Hydrophobic amino acids surrounding the phenyl ring of FK-A5 in the PI3K–FK-A5 complex.

our previous experimental study[4] indicate that the PI3K inhibitory activity of FK-A5 is higher than that of romidepsin. The differences in the hydrogen bonding patterns between romidepsin and FK-A5 may cause the different inhibitory activities in these compounds. Only one hydrogen bond was common to both the PI3K–romidepsin and PI3K–FK-A5 complexes, which occurred between a hydroxyl group in the side chain of Ser774 and an adjacent amide oxygen of the 21-isopropyl in the ligand molecules (that is, the O1 atoms shown in Fig. 1). As previously mentioned, the atoms around the 21-isopropyl have been indicated as important for the formation of complexes between PI3K and its inhibitors, because these atoms are located in the similar positions for both romidepsin and FK-A5 in their predicted docking poses. The hydrogen bond formation between the O1 atom and Ser774 supports the importance of the moiety around 21-isopropyl. Mandelker et al. reported that a large conformational change of the loop (772–777) was observed due to the binding of the PI3K inhibitor wortmannin to p110α [19], indicating that the loop (772–777) plays an important role in ligand binding. Thus, the hydrogen bond between Ser774 and PI3K inhibitors may be significant to the inhibitory activities of romidepsin and its analogs. A detailed discussion of hydrogen bonding is included with the discussion of the results of the MD simulations. The hydrophobic residues located within 4.0 Å of the phenyl ring of FK-A5 in the predicted PI3K–FK-A5 complex structure are shown in Fig. 5. As shown in the figure, the phenyl ring was surrounded by hydrophobic residues, and the binding affinities between PI3K and romidepsin or its analogs seem to be influenced by the hydrophobic effect of this position. For romidepsin and FK-A5, the different moieties were located in this area of the PI3K kinase pocket, i.e., 4-isopropyl and 7-benzyl for romidepsin and FK-A5, respectively. The difference of size between the isopropyl and benzyl groups may cause the difference of the hydrophobic effects, which may underlie the different binding affinities of romidepsin and FK-A5. In addition, the 7-benzyl of FK-A5 is a π system, while the 4-isopropyl of romidepsin is not. Thus, π–π interactions between FK-A5 and the residues of the aromatic ring, i.e., Trp780, Phe930 and Tyr836, may be expected. Both entropic hydrophobic effects and enthalpic π–π interactions may increase the binding affinity of FK-A5 over that of romidepsin. However, the 21-isopropyl, which is a highly superposed moiety between romidepsin and FK-A5, was located at the edge of the cavity, with only one hydrophobic residue (Ala775) present nearby. This

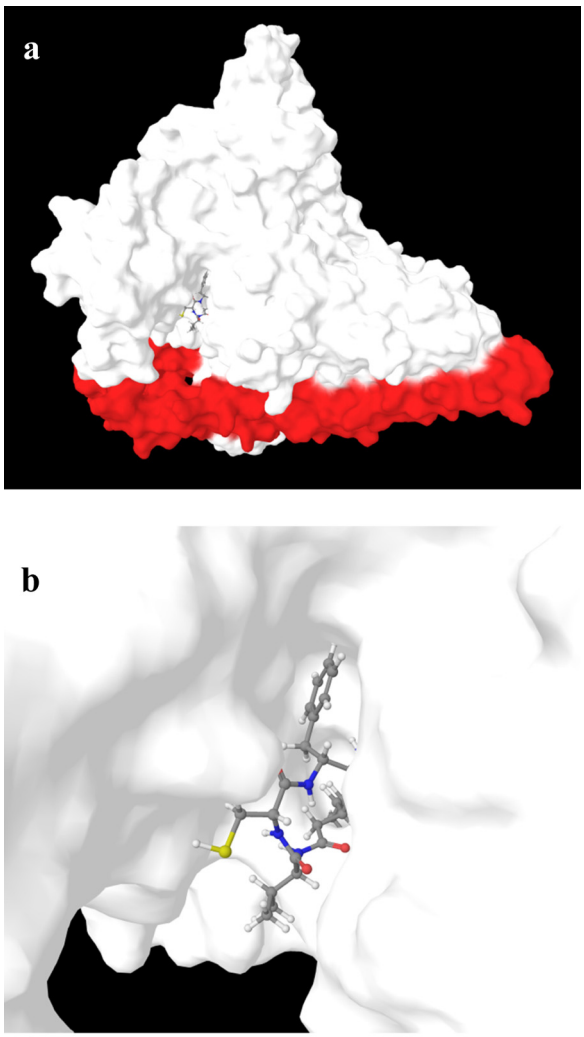

Fig. 6. Protein surface and docked ligand for the PI3K–FK-A5 complex.

observation suggests that the hydrophobic effects for the 21-isopropyl are small, or possibly negligible. Although the atoms adjacent to the 21-isopropyl were important for ligand binding, as previously discussed, the 21-isopropyl itself may be not important to PI3K-inhibitor interactions. Thus, the substitution of the 21-isopropyl with a larger substituent that interacts with PI3K may increase the binding affinity between PI3K and its inhibitors.

The protein surface of the PI3K–FK-A5 complex is illustrated in Fig. 6. The surface shown in Fig. 6 represents the solvent-accessible surface with a probe radius of 1.4 Å. In the figure, the surface of p110α is colored white, and that of p85α is illustrated as red. FK-A5 is shown by a ball-and-stick model colored by element. As shown in the figure, although FK-A5 was located deep inside the kinase pocket of p110α, the 21-isopropyl was located at the edge of the pocket and was exposed to the water solvent. Fig. 6 supports the hypothesis previously discussed, in which another moiety may be substituted for the 21-isopropyl if the hydrogen bonding pattern shown in Fig. 4 can be preserved. Additionally, extra space exists around the benzyl group of FK-A5 in the cavity of p110α, and the substitution of the benzyl group by a larger substituent may improve the binding affinity between PI3K and the inhibitor. For example, the substitution of the benzyl group by a larger aromatic system may improve the binding affinity because the π–π interactions between the inhibitor and the residues with aromatic rings would be expected to increase. The modification strategy for

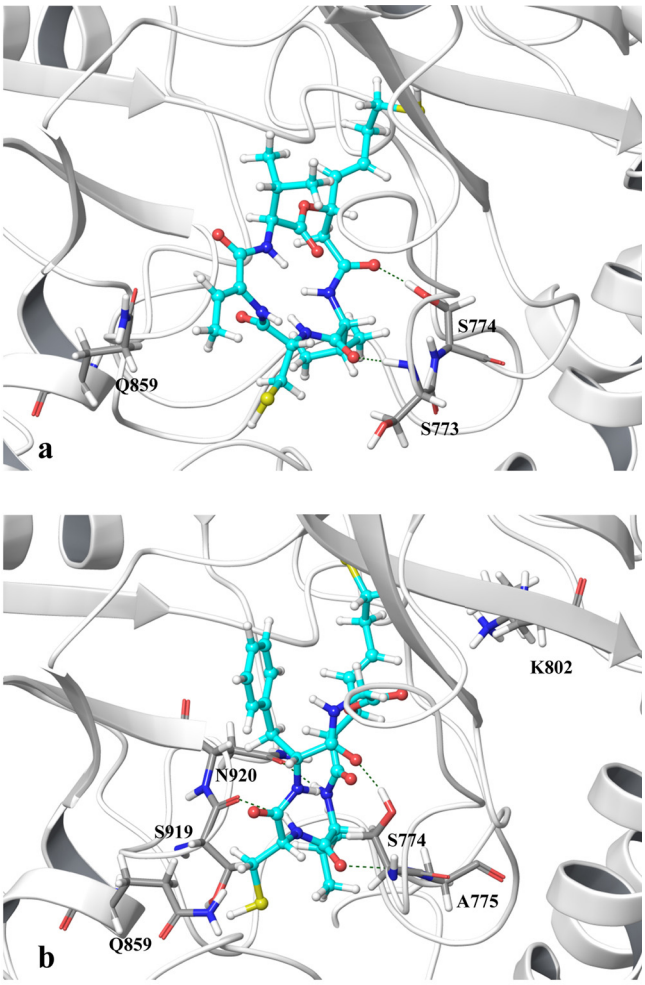

Fig. 7. Hydrogen bonds between PI3K and the ligands in the complexes after the MD simulations. The green dashed lines indicate the hydrogen bonds. (a) PI3K-romidepsin (b) PI3K–FK-A5 complexes. (For interpretation of the references to color in this figure legend, the reader is referred to the web version of this article.)

romidepsin is comparable to that for FK-A5, because the selected docking poses of romidepsin and FK-A5 were similar to each other, as shown in Fig. 3b.

In this study, MD simulations of the predicted 3D structures of the PI3K-inhibitor complexes were conducted for structural refinement. The root mean square deviations (RMSDs) for the main chain atoms were calculated along the MD trajectories. In the last 4 ns of the MD simulations, the average RMSDs were 2.96 Å and 2.64 Å for the PI3K-romidepsin and PI3K–FK-A5 complexes, respectively. The standard deviations of the RMSDs were 0.188 Å and 0.106 Å for the PI3K-romidepsin and PI3K–FK-A5 complexes, respectively. These results indicate the convergence of the MD simulations of the PI3K–inhibitor complexes. The hydrogen bonds between PI3K and its inhibitors observed after the MD simulations are illustrated in Fig. 7. As shown in the figure, Ser774 remained important to the hydrogen bonding between PI3K and the inhibitors for both romidepsin and FK-A5 after the MD simulations. For romidepsin, the hydrogen bond acceptor for Ser774 was the amide oxygen atom adjacent to the 21-isopropyl (O1 in Fig. 1) both before and after the MD simulations. Conversely, for FK-A5, the hydrogen bond acceptor for Ser774 was the amide oxygen adjacent to the benzyl group (O5 in Fig. 1) after the MD simulation, although the O1 atom was the acceptor before the MD simulation. However, the distance between O1 in FK-A5 and the hydroxyl hydrogen in Ser774 was only 3.63 Å after the MD simulation. Although this distance exceeded the definition of hydrogen bond used in this study, these atoms were enough close to interact. In addition, the distance between the O5 in FK-A5 and the hydroxyl hydrogen in Ser774 was 3.59 Å before the MD simulation. That is, the bifurcated hydrogen bond [30] between O1···Ser774···O5 may have formed and existed stably during the MD simulation. Thus, the bifurcated hydrogen bond likely plays an important role in the binding affinity of FK-A5, and the results support the hypothesis that Ser774 is important for the recognition of romidepsin and its analogs by PI3K. In addition to the hydrogen bonds with Ser774, other hydrogen bonds between PI3K and the inhibitors were observed for both the PI3K-romidepsin and PI3K–FK-A5 complexes. For romidepsin, although only one hydrogen bond with Ser774 was observed before the MD simulation, the hydrogen bond between the O3 in romidepsin and the amide hydrogen of Ser773 in PI3K was formed after the structural relaxation of the MD simulation. For FK-A5, the two hydrogen bonds that were observed before the MD simulations, Lys802···O4 and Gln859···O2, disappeared after the MD simulations, while three new hydrogen bonds, Ala775···O3, Ser919···H-N2 and Asn920···H-N1, were observed after the process. The number of hydrogen bonds for FK-A5 was larger than that for romidepsin even after the MD simulations, although the residues involved in the hydrogen bonds were different before and after the simulations. These hydrogen bonding tendencies may influence the binding affinities of the PI3K inhibitors. Because Lys802 formed a salt bridge with Asp810 after the MD simulation, the hydrogen bond between Lys802 and FK-A5 disappeared. Mandelker et al. reported that Lys802 formed a covalent bond with wortmannin [19]. Because the 3D structure of the PI3K–wortmannin complex (PDB ID: 3HHM) was used for these docking calculations, the interaction between Lys802 and FK-A5 may be overestimated, and the predicted complex structure may be influenced by the 3HHM structure before the MD simulation. In addition, Gln859, for which the hydrogen bond disappeared after the MD simulation, was exposed to the water solvent in the MD-relaxed structure calculated using the explicit water solvent. These results indicate that the structural refinements obtained using MD simulations with explicit water are useful for removing the artifacts in the predicted structures of complexes as calculated by docking trials. After the MD simulation of the PI3K–FK-A5 complex, three hydrogen bonds were observed: between the amide hydrogen of Ala775 and the O3 of FK-A5, between the hydroxyl oxygen of Ser919 and the N2 hydrogen of FK-A5, and between the oxygen in the side chain of Asn920 and the N1 hydrogen of FK-A5. The orientations of Ala775 and Ser919 were originally appropriate for the formation of hydrogen bonds, although the distances were relatively large before the MD simulations (Ala775···O3 was 5.04 Å and Ser919···H-N2 was 4.21 Å). After the structural refinements obtained using MD simulation, the residues were rearranged to feasible positions for hydrogen bond formation. Conversely, the amide group of the side chain in Asn920 was rotated to form a hydrogen bond with FK-A5 after MD simulation. That is, nearly hydrogen-bonding structures were originally obtained by the docking calculations for these residues, and the 3D structures were then refined using the MD simulations. A hydrogen bond between Ser773 and romidepsin, as well as between Ala775 and FK-A5, were also observed after the MD simulations. Because both Ser773 and Ala775 were located in the loop (772–777), these results were consistent with experimental results in which the loop (772–777) was related to ligand binding.

In Tables 1 and 2, the occurrence rates of the hydrogen bonds between PI3K and the two inhibitors during the MD simulations are shown. The occurrence rates were calculated for the last 4 ns of the MD simulations. Table 1 displays the results for the PI3K–romidepsin complex, and Table 2 displays those for the PI3K–FK-A5 complex. Only those hydrogen bonds with occurrence

Table 1
Hydrogen bond frequencies during the MD simulations of the PI3K-romidepsin complex.

	Acceptor	Donor	Frequency (%)
1	Romidepsin@O3	Ser773@N	47.9
2	Romidepsin@O5	Val851@N	24.8
3	Romidepsin@O2	Gln859@Nε2	5.8
4	Romidepsin@O1	Ser774@Oγ	5.0

Table 2
Hydrogen bond frequencies during the MD simulations of the PI3K–FK-A5 complex.

	Acceptor	Donor	Frequency (%)
1	FK-A5@O5	Ser774@Oγ	99.3
2	Asn920@Oδ1	FK-A5@N1	83.9
3	FK-A5@O3	Ala775@N	79.8
4	Ser919@O	FK-A5@N2	44.2

rates of 5.0% or greater are shown in these tables. A distance threshold of 3.5 Å and an angle threshold of 120° were used to define the hydrogen bond in considering the fluctuation of the MD simulation at 300 K. The hydrogen bonding analyses were conducted using the cpptraj module of AMBER12 [28]. The hydrogen bonds shown in these tables are illustrated in Fig. 7, except for hydrogen bonds **2** and **3** in Table 1. Val851 was located in the hydrophobic region shown in Fig. 5, and additional space existed in the region. Thus, the fluctuation of the location and the conformation of Val851 caused hydrogen bond **2** in 24.8% of the MD trajectories. Although hydrogen bond **3** was not observed in the final structure of the MD simulation shown in Fig. 7, it was observed in 5.8% of the MD trajectories because of the flexible side chain of Gln859. As shown in the tables, the frequencies of the hydrogen bond formations were greater for FK-A5 than for romidepsin. The occurrence rates of all hydrogen bonds were less than 50% in romidepsin, while three hydrogen bonds occurred in 70% of the MD trajectories for FK-A5. These results suggest that the differences in the hydrogen bonding frequencies cause the difference of the inhibitory activities between romidepsin and FK-A5.

The MD simulation of the PI3K–wortmannin complex, whose X-ray structure has previously been determined [19], was performed, and the hydrogen bonding pattern of PI3K–wortmannin was compared with those of the PI3K–romidepsin and PI3K–FK-A5 complexes. The structure of wortmannin is illustrated in Fig. 8, and the occurrence rates of hydrogen bonds in the PI3K–wortmannin complex during the MD simulation are shown in Table 3. As mentioned above, wortmannin is covalently bonded to the Lys802 of PI3K. Thus, hydrogen bond **1** in Table 3 was located near the covalent bond between wortmannin and Lys802 and seems to play only

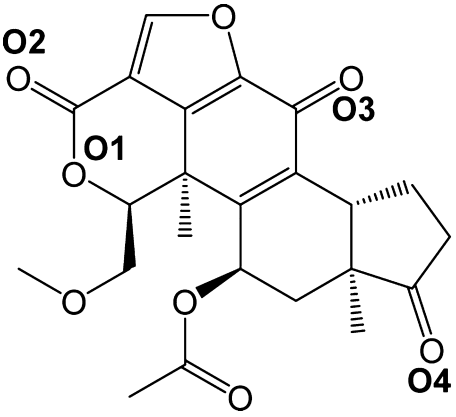

Fig. 8. PI3K inhibitor wortmannin.

Table 3
Hydrogen bond frequencies during the MD simulations of the PI3K–wortmannin complex.

	Acceptor	Donor	Frequency (%)
1	Wortmannin@O2	Lys802@Nζ	97.2
2	Wortmannin@O4	Val851@N	92.2
3	Wortmannin@O3	Tyr836@Oη	72.1
4	Wortmannin@O2	Ser774@Oγ	48.5
5	Wortmannin@O1	Ser774@Oγ	41.7
6	Wortmannin@O3	Asp933@N	13.7

a minor role in ligand recognition. Conversely, hydrogen bonds **3** and **4** were formed between wortmannin and Ser774, which was among the most important residues in the ligand recognition of the PI3K-romidepsin and PI3K–FK-A5 complexes. Furthermore, because the hydrogen donor of hydrogen bonds **3** and **4** was the same atom, i.e., Oγ of Ser774, the bifurcated hydrogen bond likely plays an important role in the interaction between PI3K and wortmannin. These results suggest that Ser774 is the conserved interaction hotspot in the binding site of PI3K.

In addition to the hydrogen bonding patterns, the locations of hydrophobic residues in the complex structures obtained by the MD simulations were investigated. Hydrophobic effects between PI3K and its inhibitors were observed in the complex structures both before and after the MD simulations. Before the MD simulations, only one hydrophobic residue (Ala775) was located near the 21-isopropyl of romidepsin. After the MD simulations, Ala775 moved away from the 21-isopropyl, and Ile1058 was instead located near this residue. For the PI3K–FK-A5 complex, Ala775 and Phe1059 were located near the 21-isopropyl of FK-A5 after the MD simulations; therefore, only one additional hydrophobic residue was observed. For both romidepsin and FK-A5, 21-isopropyl was exposed to the water solvent. These results suggest that the hydrophobic effects of the 21-isopropyl are small, as is consistent with the docking results. Conversely, the number of hydrophobic residues around the 7-benzyl group of FK-A5 increased after the MD simulations. Only one residue shown in Fig. 5 moved away from the 7-benzyl in the MD simulations (Phe930), and three additional hydrophobic residues, i.e., Met772, Ile800, and Ile848, were located near the 7-benzyl moiety. Even for Phe930, the distance from the 7-benzyl was approximately 4.5 Å. For the PI3K–romidepsin complex, two additional residues, i.e., Met772 and Ile800, were located near the 4-isopropyl group of romidepsin after the MD simulations. These results indicate that the hydrophobic effects of this region play an important role in the ligand recognition of PI3K and that these hydrophobic contacts are refined by MD simulations.

In addition to the interaction analyses, binding affinity calculations by the MM/GBSA method were carried out. The calculated binding free energy between PI3K and romidepsin was −28.8637 kcal/mol, and that between PI3K and FK-A5 was −38.7268 kcal/mol. As mentioned above, hydrogen bonding patterns and hydrophobic effects were consistent with the experimental inhibitory activities of inhibitors, and the calculated binding free energies also indicate the higher activity of FK-A5. The results suggest that the predicted structures of PI3K–inhibitor complexes are reasonable and the prediction strategies used in this study are useful for the protein–ligand complex structures.

4. Conclusions

In this study, the 3D structures of the complexes between PI3K and two inhibitors, romidepsin and its analog FK-A5, were predicted. For these predictions, a combination of computational docking, representing an SBDD method, and molecular superposition, representing an LBDD method, was employed. Reasonable structures for the complexes were obtained using this combination

and could explain the difference of the inhibitory activities between romidepsin and FK-A5. The predicted structures of the complexes suggest that a larger hydrophobic substituent, especially a larger aromatic moiety, at the 7-position would increase binding affinity in romidepsin and its analog due to the enhancement of the hydrophobic effect and/or π–π interactions. The occurrence rates of hydrogen bonds for FK-A5 were also greater than those for romidepsin, as was consistent with the difference of the inhibitory activities between the two compounds. These results indicate that the combination of SBDD and LBDD is a powerful method for predicting the structures of complexes between drug targets and large ligand molecules, including those with macrocycles. In addition, the structural refinements obtained using MD simulations are useful for predicting the interactions between proteins and ligands.

In this study, a modification strategy for increasing the binding affinity of romidepsin and its analogs through substitutions at the 7- and 21-positions was proposed. Using these results, improved HDAC/PI3K dual inhibitors with higher inhibitory activities for PI3K may be developed. The modifications of these compounds are currently being conducted.

Acknowledgements

Parts of the computations were performed by the Research Center for Computational Science, Okazaki. This work was supported by a grant-in-aid for scientific research [23790137] from the Japan Society for the Promotion of Science.

References

[1] D.A. Fruman, R.E. Meyers, L.C. Cantley, Phosphoinositide kinases, Annu. Rev. Biochem. 67 (1998) 481–507.
[2] Y. Samuels, Z. Wang, A. Bardelli, N. Silliman, J. Ptak, S. Szabo, H. Yan, A. Gazdar, S.M. Powell, G.J. Riggins, J.K.V. Willson, S. Markowitz, K.W. Kinzler, B. Vogelstein, V.E. Velculescu, High frequency of mutations of the PIK3CA gene in human cancers, Science 304 (2004) 554.
[3] D. Kong, T. Yamori, Advances in development of phosphatidylinositol 3-kinase inhibitors, Curr. Med. Chem. 16 (2009) 2839–2854.
[4] K. Saijo, T. Katoh, H. Shimodaira, A. Oda, O. Takahashi, C. Ishioka, Romidepsin (FK228) and its analogs directly inhibit PI3K activity and potently induce apoptosis as HDAC/PI3K dual inhibitors, Cancer Sci. 103 (2012) 1994–2001.
[5] H. Ueda, H. Nakajima, Y. Hori, T. Fujita, M. Nishimura, T. Goto, M. Okuhara, FR901228, a novel antitumor bicyclic depsipeptide produced by *Chromobacterium violaceum* No. 968. I. Taxonomy, fermentation, isolation, physico-chemical and biological properties, and antitumor activity, J. Antibiot. 47 (1994) 301–310.
[6] R. Furumai, A. Matsuyama, N. Kobashi, K.H. Lee, M. Nishiyama, H. Nakajima, A. Tanaka, Y. Komatsu, N. Nishino, M. Yoshida, S.S. Horinouchi, FK228 (depsipeptide) as a natural prodrug that inhibits class I histone deacetylases, Cancer Res. 62 (2002) 4916–4921.
[7] J.S. Carew, F.J. Giles, S.T. Nawrocki, Histone deacetylase inhibitors: mechanisms of cell death and promise in combination cancer therapy, Cancer Lett. 269 (2008) 7–17.
[8] A.C. West, R.W. Johnstone, New and emerging HDAC inhibitors for cancer treatment, J. Clin. Invest. 124 (2014) 30–39.
[9] M.B. Wozniak, R. Villuendas, J.R. Bischoff, C.B. Aparicio, J.F. Martínez Leal, P. de La Cueva, M.E. Rodriguez, B. Herreros, D. Martin-Perez, M.I. Longo, M. Herrera, M.A. Piris, P.L. Ortiz-Romero, Vorinostat interferes with the signaling transduction pathway of T-cell receptor and synergizes with phosphoinositide-3 kinase inhibitors in cutaneous T-cell lymphoma, Haematologica 95 (2010) 613–621.
[10] K. Ozaki, M. Kosugi, N. Baba, K. Fujio, T. Sakamoto, S. Kimura, S. Tanimura, M. Kohno, Blockade of the ERK or PI3K-Akt signaling pathway enhances the cytotoxicity of histone deacetylase inhibitors in tumor cells resistant to gefitinib or imatinib, Biochem. Biophys. Res. Commun. 391 (2010) 1610–1615.
[11] C. Zhou, L. Qiu, Y. Sun, S. Healey, H. Wanebo, N. Kouttab, W. Di, B. Yan, Y. Wan, Inhibition of EGFR/PI3K/AKT cell survival pathway promotes TSA's effect on cell death and migration in human ovarian cancer cells, Int. J. Oncol. 26 (2006) 269–278.
[12] S. Wilhelm, C. Carter, M. Lynch, T. Lowinger, J. Dumas, R.A. Smith, B. Schwartz, R. Simantov, S. Kelley, Discovery and development of sorafenib: a multikinase inhibitor for treating cancer, Nat. Rev. Drug Discovery 5 (2006) 835–844.
[13] P.J. Gane, P.M. Dean, Recent advances in structure-based rational drug design, Curr. Opin. Struct. Biol. 10 (2000) 401–404.
[14] D.B. Kitchen, H. Decornez, J.R. Furr, J. Bajorath, Docking and scoring in virtual screening for drug discovery: methods and applications, Nat. Rev. Drug Discovery 3 (2004) 935–949.
[15] A. Oda, K. Tsuchida, T. Takakura, N. Yamaotsu, S. Hirono, Comparison of consensus scoring strategies for evaluating computational models of protein–ligand complexes, J. Chem. Inf. Model. 46 (2006) 380–391.
[16] K. Yasuo, N. Yamaotsu, H. Gouda, H. Tsujishita, S. Hirono, Structure-based CoMFA as a predictive model—CYP2C9 inhibitors as a test case, J. Chem. Inf. Model. 49 (2009) 853–864.
[17] C. Acharya, A. Coop, J.E. Polli, A.D. MacKerell Jr., Recent advances in ligand-based drug design: relevance and utility of the conformationally sampled pharmacophore approach, Curr. Comput. Aided Drug Des. 7 (2011) 10–22.
[18] H.M. Berman, J. Westbrook, Z. Feng, G. Gilliland, T.N. Bhat, H. Weissig, I.N. Shindyalov, P.E. Bourne, The protein data bank, Nucleic Acids Res. 28 (2000) 235–242.
[19] D. Mandelker, S.B. Gabelli, O. Schmidt-Kittler, J. Zhu, I. Cheong, C.H. Huang, K.W. Kinzler, B. Vogelstein, L.M. Amzel, A frequent kinase domain mutation that changes the interaction between PI3Kα and the membrane, Proc. Natl. Acad. Sci. U.S.A. 106 (2009) 16996–17001.
[20] M.J. Frisch, G.W. Trucks, H.B. Schlegel, G.E. Scuseria, M.A. Rob, J.R. Cheeseman, J.A. Montgomery Jr., T. Vreven, K.N. Kudin, J.C. Burant, J.M. Millam, S.S. Iyengar, J. Tomasi, V. Barone, B. Mennucci, M. Cossi, G. Scalmani, N. Rega, G.A. Petersson, H. Nakatsuji, M. Hada, M. Ehara, K. Toyota, R. Fukuda, J. Hasegawa, M. Ishida, T. Nakajima, Y. Honda, O. Kitao, H. Nakai, M. Klene, X. Li, J.E. Knox, H.P. Hratchian, J.B. Cross, V. Bakken, C. Adamo, J. Jaramillo, R. Gomperts, R.E. Stratmann, O. Yazyev, A.J. Austin, R. Cammi, C. Pomelli, J.W. Ochterski, P.Y. Ayala, K. Morokuma, G.A. Voth, P. Salvador, J.J. Dannenberg, V.G. Zakrzewski, S. Dapprich, A.D. Daniels, M.C. Strain, O. Farkas, D.K. Malick, A.D. Rabuck, K. Raghavachari, J.B. Foresman, J.V. Ortiz, Q. Cui, A.G. Baboul, S. Clifford, J. Cioslowski, B.B. Stefanov, G. Liu, A. Liashenko, P. Piskorz, I. Komaromi, R.L. Martin, D.J. Fox, T. Keith, M.A. Al-Laham, C.Y. Peng, A. Nanayakkara, M. Challacombe, P.M.W. Gill, B. Johnson, W. Chen, M.W. Wong, C. Gonzalez, J.A. Pople, Gaussian 03, Gaussian, Inc., Wallingford, CT, 2003.
[21] M. McGann, FRED pose prediction and virtual screening accuracy, J. Chem. Inf. Model. 51 (2011) 578–596.
[22] OpenEye Scientific Software, Inc., OMEGA 2.4.6, OpenEye Scientific Software, Inc., Santa Fe, NM, 2012.
[23] I. Kolossváry, W.C. Guida, Low mode search. An efficient, automated computational method for conformational analysis: application to cyclic and acyclic alkanes and cyclic peptides, J. Am. Chem. Soc. 118 (1996) 5011–5019.
[24] J. Wang, R.M. Wolf, J.W. Caldwell, P.A. Kollman, D.A. Case, Development and testing of a general AMBER force field, J. Comput. Chem. 25 (2004) 1157–1174.
[25] OpenEye Scientific Software, Inc., ROCS 3.1.2, OpenEye Scientific Software, Inc., Santa Fe, NM, 2011.
[26] J. Wang, P. Cieplak, P.A. Kollman, How well does a restrained electrostatic potential (RESP) model perform in calculating conformational energies of organic and biological molecules? J. Comput. Chem. 21 (2000) 1049–1074.
[27] V. Hornak, R. Abel, A. Okur, B. Strockbine, A. Roitberg, C. Simmerling, Comparison of multiple Amber force fields and development of improved, Proteins: Struct., Funct., Bioinf. 65 (2006) 712–725.
[28] D.A. Case, T.A. Darden, T.E.T.E. Cheatham III, C.L. Simmerling, J. Wang, R.E. Duke, R. Luo, R.C. Walker, W. Zhang, K.M. Merz, B. Roberts, S. Hayik, A. Roitberg, G. Seabra, J. Swails, A.W. Goetz, I. Kolossváry, K.F. Wong, F. Paesani, J. Vanicek, R.M. Wolf, J. Liu, X. Wu, S.R. Brozell, T. Steinbrecher, H. Gohlke, Q. Cai, X. Ye, J. Wang, M.J. Hsieh, G. Cui, D.R. Roe, D.H. Mathews, M.G. Seetin, R. Salomon-Ferrer, C. Sagui, V. Babin, T. Luchko, S. Gusarov, A. Kovalenko, P.A. Kollman, AMBER 12, University of California, San Francisco, San Francisco, CA, 2012.
[29] K.E. Cole, D.P. Dowling, M.A. Boone, A.J. Phillips, D.W. Christianson, Structural basis of the antiproliferative activity of largazole, a depsipeptide inhibitor of the histone deacetylases, J. Am. Chem. Soc. 133 (2011) 12474–12477.
[30] I. Rozas, I. Alkorta, J. Elguero, Bifurcated hydrogen bonds: three-centered interactions, J. Phys. Chem. A 102 (1998) 9925–9932.